Presented at the COMSOL Conference 2009 Boston

MODELING CONTACT LINE DYNAMICS IN EVAPORATING MENISCI

J. L. Plawsky, A. Chatterjee, and P. C. Wayner, Jr.

Department of Chemical and Biological Engineering,
Rensselaer Polytechnic Institute, Troy, NY-12180

Introduction: Phase Change Heat Transfer

The efficient acquisition and rejection of heat at very high heat fluxes (kW/cm^2) requires synergistic advances in heat transfer materials, heat transfer surfaces, and heat transfer devices

Electronics cooling

Photonics cooling

Space & Aviation

Solar Energy

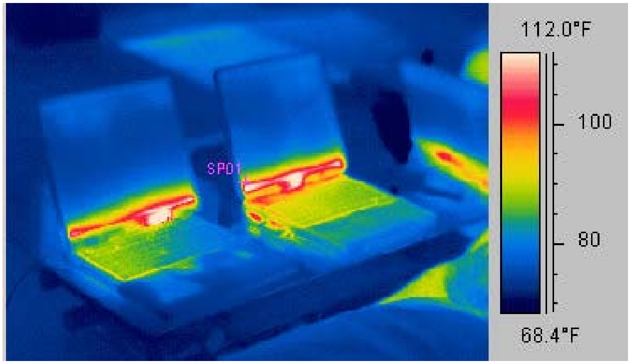

Various other applications include:

Coating, Plating, Cooling, Separation and Reaction, Adhesion, Boiling and Condensation, Fuel Cell, Gas Sensor (porous coatings), Heat and Mass Transfer Operations & Self-Assembly.

Evaporation from Transition Region

Evaporation occurs in the region which has the lowest total resistance to heat transfer.

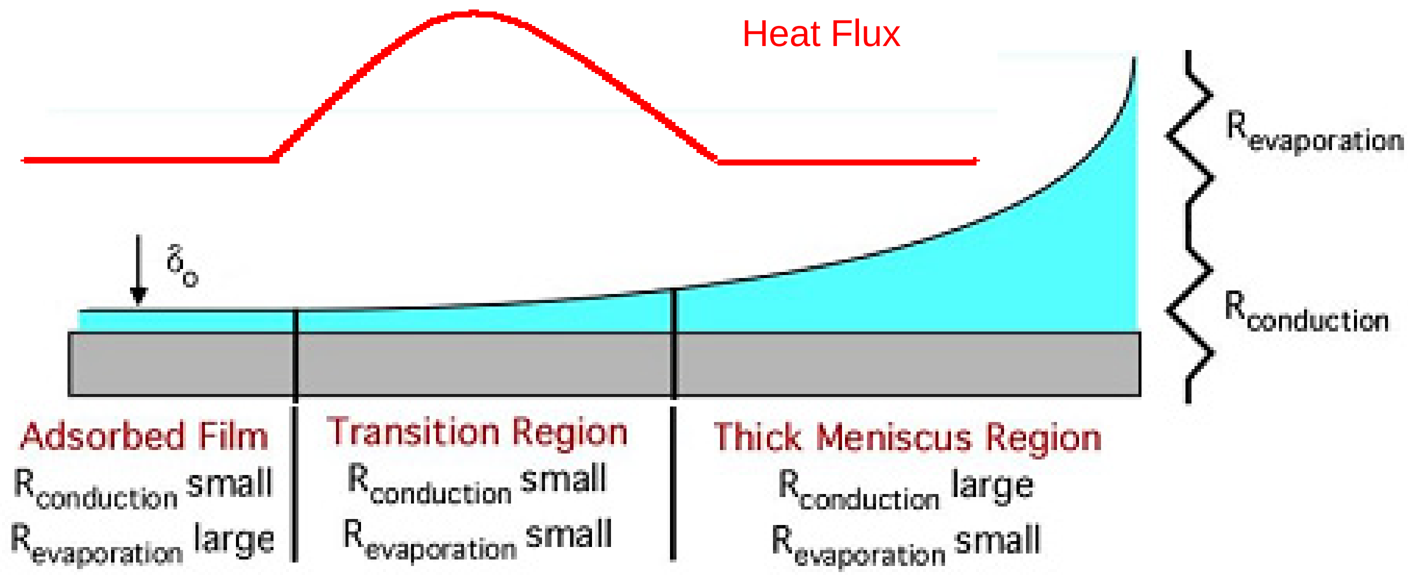

Transition region controls evaporation. <u>Goal is to maximize its extent.</u>

– Accurate modeling will enable us to engineer optimal surfaces

Experimental System - Heat Pipes

ISS CVB Module

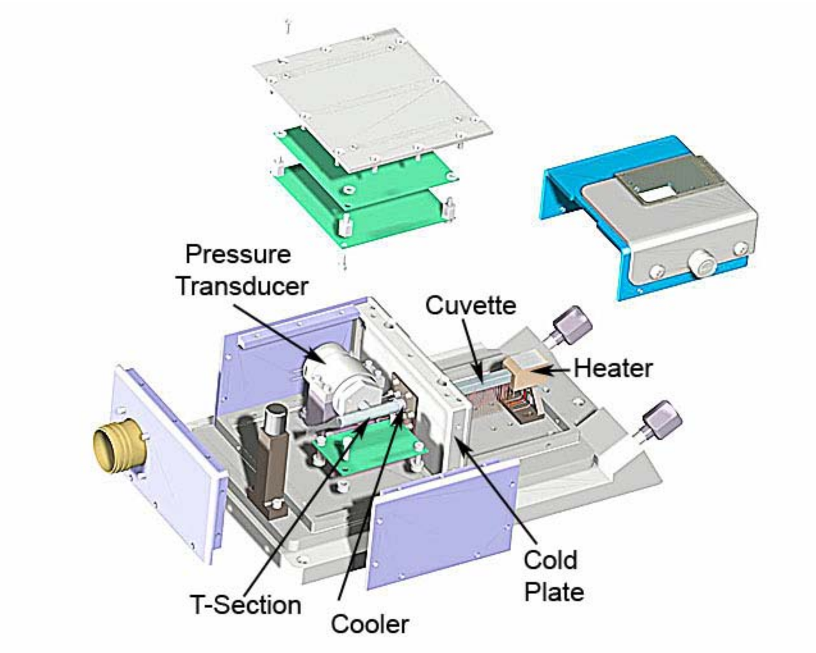

Photograph of Module

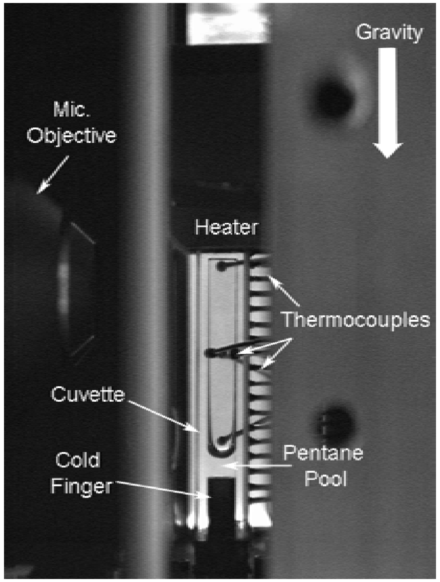

- Partially filled cell forms a Constrained Vapor Bubble (CVB) design.
- Meniscus is present at corners where surface and the base meet
- Forms the basis for a fundamental experiment in interfacial phenomena
- Can be operated isothermally or driven by a temperature gradient

Reflectivity/Interferometry Technique

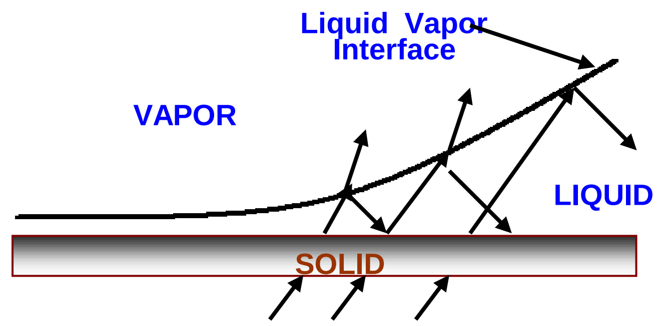

Varying thickness of the meniscus produces an interference pattern

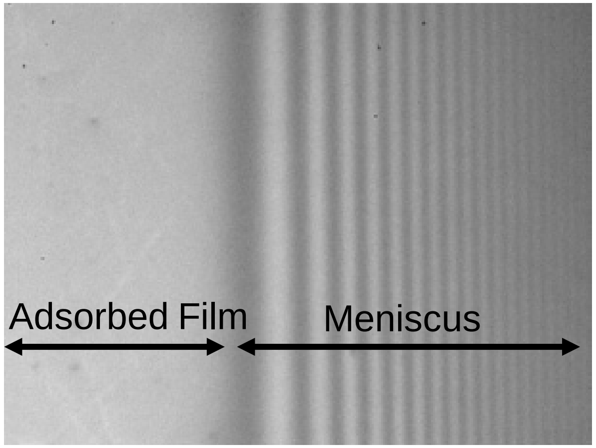

Interference pattern analyzed to obtain gray value at each pixel

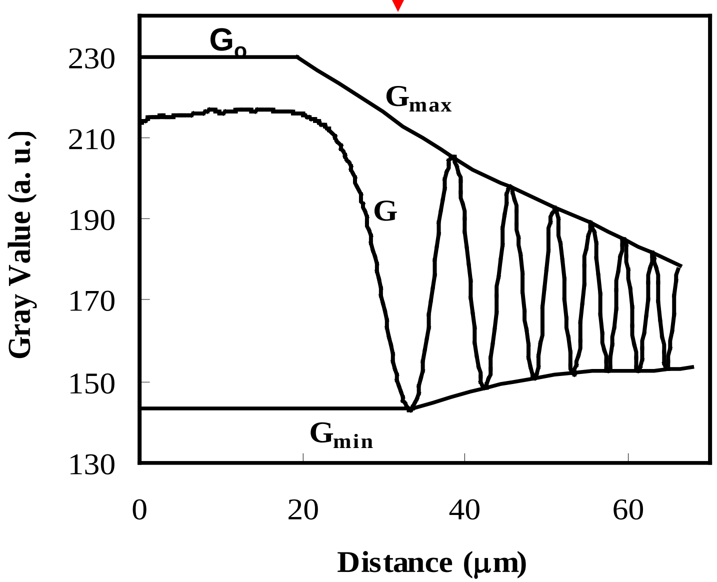

$$\overline{G}(x) = \frac{G(x) - G_{\min}(x)}{G_{\max}(x) - G_{\min}(x)}$$

$$RL(x) = \overline{G}(x)\left[RL_{\max} - RL_{\min} \right] + RL_{\min}$$

$$RL(x) = \frac{\alpha + \beta \cos 2\phi_l(\delta)}{\kappa + \beta \cos 2\phi_l(\delta)}$$

Nonisothermal State Meniscus - Octane

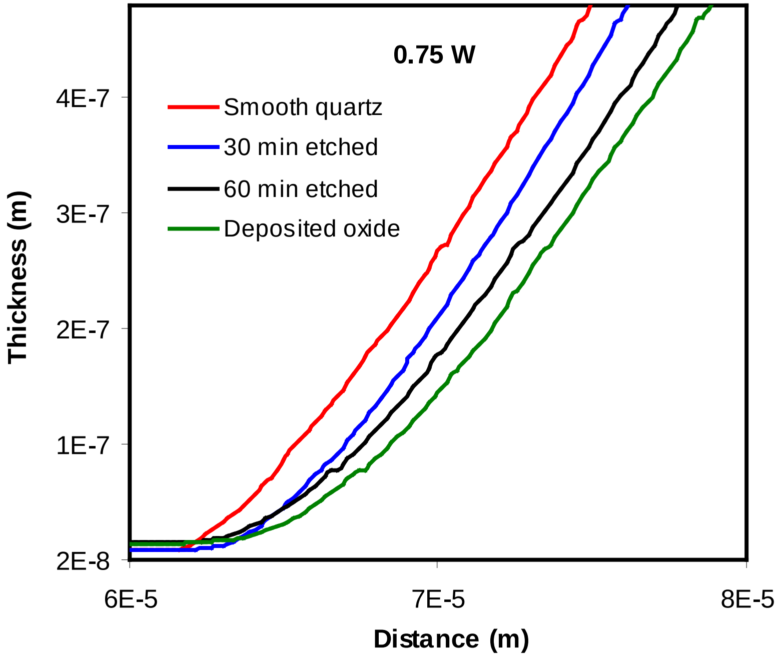

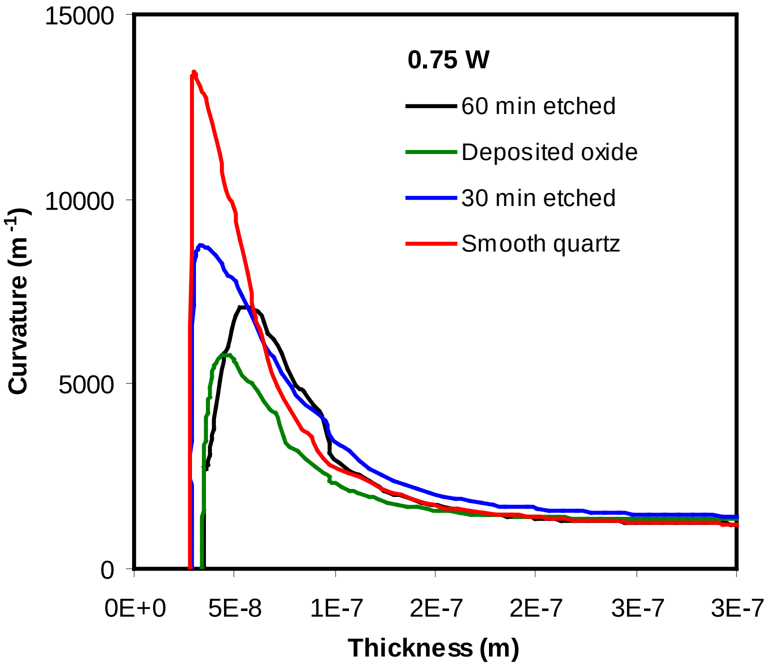

Octane (8-C) used as a working fluid

Table 3.1: Physical properties of n-pentane and n-octane

	Dielectric Constant, ε	Refractive index, n	Boiling point, °C	Surface Tension, σ, dynes/cm	Dynamic Viscosity, $\times 10^3$ Pas	Density, ρ, Kg/m^3	h_{fg}, kJ/kg
Pentane	1.84	1.358	36	15.5	0.224	626	366
Octane	1.95	1.398	126	21.1	0.508	703	363

Fluid Flow Model

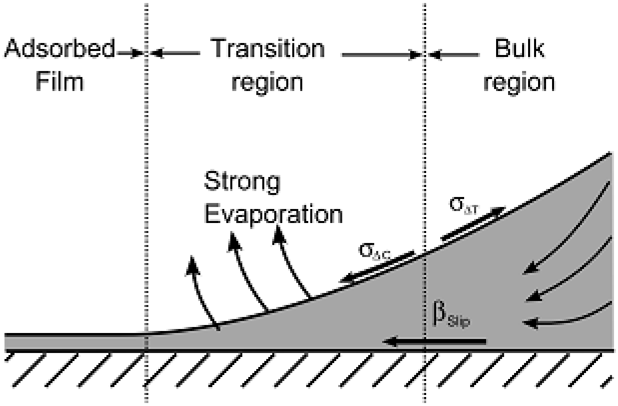

- Lubrication approximation used to model fluid flow.
- Navier slip (solid-liquid interface) and Marangoni shear (liquid-vapor interface) boundary conditions applied

- Mass balance provides the evaporating mass flux at each pixel location.
- Temperature dependence of fluid properties accounts for the capillary, Marangoni and van der Waals forces.

$$\mu \frac{d^2u}{dz^2} = \frac{dP_l}{dy}$$

$$z = 0, \qquad u_s = \beta \left.\frac{du}{dz}\right|_{z=0}$$

$$z = \delta(y), \qquad \tau_{zy} = \frac{d\sigma_{lv}}{dy}$$

$$P_l(y) = P_v - \left[\sigma(y)K(y) + \Pi(y)\right]$$

$$\Gamma = \int_0^{\delta} \rho_l u \, dy \qquad q'' = -h_{fg} \frac{d\Gamma}{dy}$$

Heat Transfer at the Contact Line

- Heat transfer at the contact line was modeled using a Kelvin-Clapeyron approach.

$$\frac{d\Gamma}{dy} = -\dot{m}_{evp} = C\left(\frac{M}{2\pi RT}\right)^{1/2}\left\{\frac{P_v M h_{fg}}{RT_v T_i}\left(T_i - T_v\right) + \frac{V_l P_v}{RT_i}\left(P_l - P_v\right)\right\}$$

$$\boxed{\begin{aligned}&\frac{1}{3\nu_1}\frac{d}{dy}\left[\left(\sigma_o - \gamma\left(T_{lv} - T_v\right)\right)\delta^3\delta''' - \gamma\delta^3\delta''\frac{dT_{lv}}{dy} + \frac{3A}{\delta}\delta' + \frac{3\gamma\delta^2}{2}\frac{dT_{lv}}{dy}\right] \\ &+\left[a\left(T_{lv} - T_v\right) - b\left(\sigma\delta'' - \gamma\left(T_{lv} - T_v\right)\delta'' - \frac{A}{\delta^3}\right)\right] = 0\end{aligned}}$$

- Since the pressure and difference can be written in terms of the film thickness, and the temperature difference is measured or set, the final equation can be written as a 4th order differential equation for the film thickness, δ.

- Boundary conditions set the film thickness and curvature at both ends of the domain.
  - These conditions are established from experimental observations.

Simulation Results

- COMSOL simulations were performed by splitting the 4th order equation into two 2nd order equations.
  - Splitting allowed for more control over boundary conditions.
  - Limited us to steady-state simulation.

- We were primarily interested in whether the model could simulate the curvature profiles we observe experimentally.

- Peak in curvature only occurs for small values of the adsorbed film thickness corresponding to high values of the disjoining pressure.

- Steep curvature gradient required to pump liquid into the transition region for evaporation.

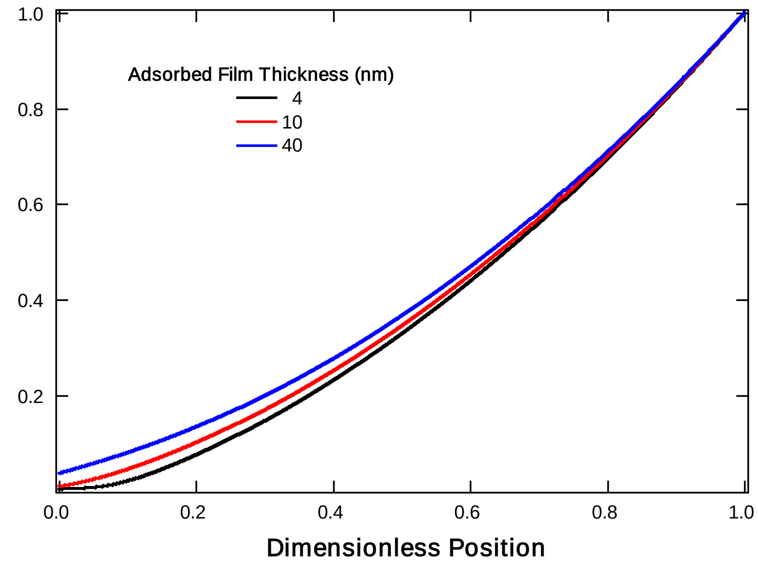

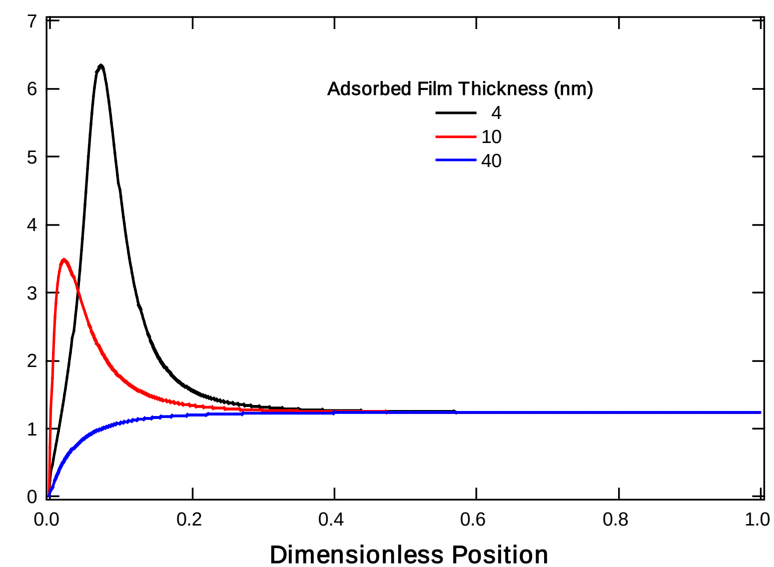

Simulation Results – Octane Low Heat Input

- COMSOL simulation was able to reproduce the experimental data from an octane meniscus.
- The incorporation of hydrodynamic slip was necessary to match both the position of the curvature peak and the spread of the peak.
- Peak height is controlled by the thickness of the adsorbed film ahead of the contact line.

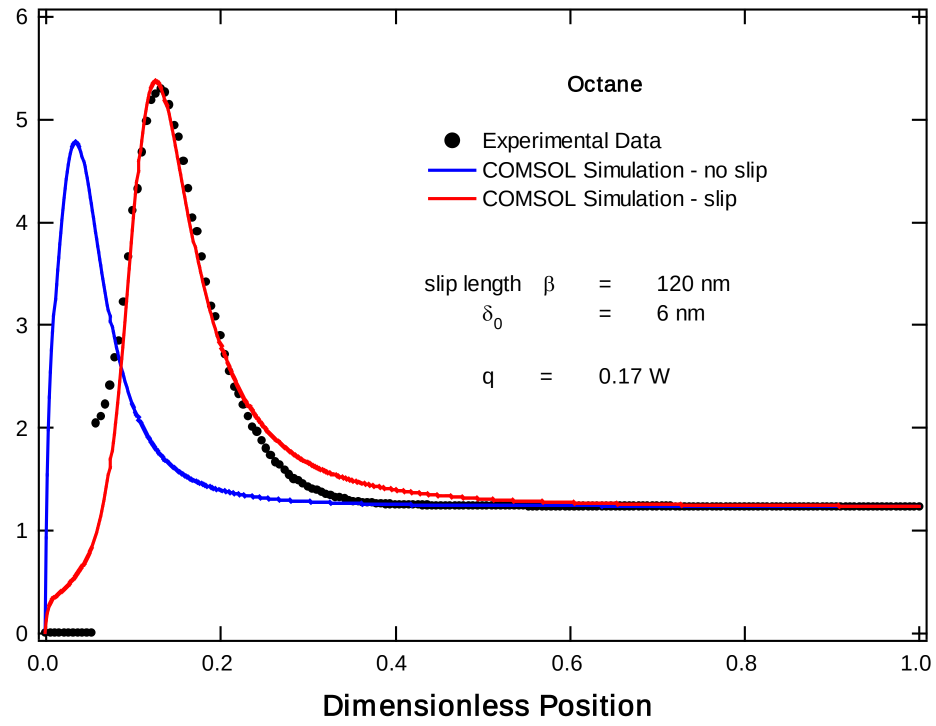

Simulation Results - Octane & Pentane

- COMSOL simulation was applied to an octane meniscus at a higher heat flux and a pentane meniscus.
- Simulation was able to successfully reproduce the curvature profiles for both fluids.
- Adsorbed film thicknesses are lower than those measured experimentally, but the trend reproduces experimental observations.
  - Pentane adsorbed film thicknesses are much larger than octane.
- Slip lengths are not unreasonably large, but more experimental work is needed to determine if they exist.

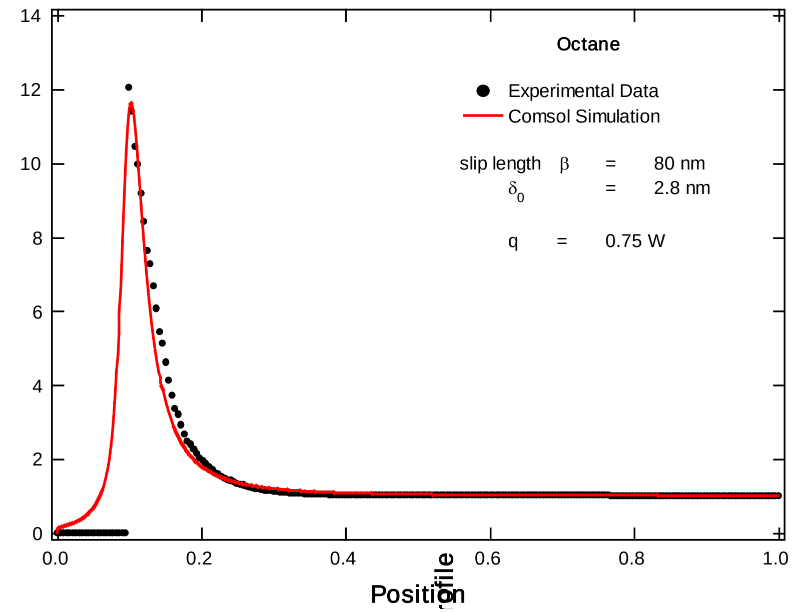

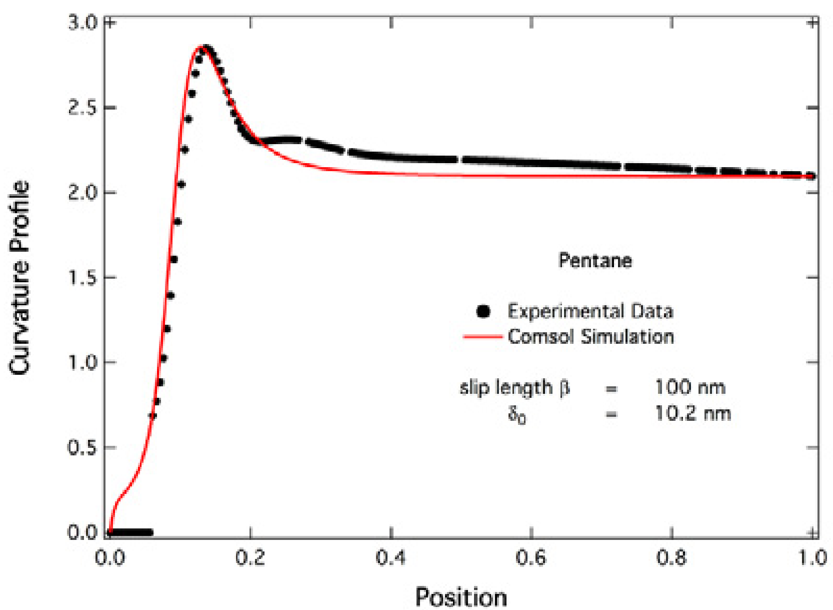

Conclusions

- **COMSOL model was successfully able to reproduce experimental observations**
  - Model was able to match both the film thickness and curvature profiles for octane and pentane menisci.
  - Model results provided the correct trend for both the adsorbed film thickness as a function of heat input and also the adsorbed film thickness as a function of liquid Hamaker constant. Adsorbed film thicknesses were smaller than those measured experimentally.
  - Model results suggest that hydrodynamic slip is required to successfully model the evaporation of thin films.

- **Meniscus model improvements**
  - Verify the requirement for a slip length.
  - Extend model to cover the entire meniscus, not just the field-of-view of the experiment.
  - Extend model to handle transient situations. Focus on recession during evaporation and meniscus oscillation, both of which have been observed experimentally.

Acknowledgements

Liftoff of Discovery with CVB Experiment
8/29/2009

Hamakar constant, Lifshitz Theory

$$A = \frac{3}{4}kT\left(\frac{\varepsilon_1 - \varepsilon_3}{\varepsilon_1 + \varepsilon_3}\right)\left(\frac{\varepsilon_2 - \varepsilon_3}{\varepsilon_2 + \varepsilon_3}\right) + \frac{3h\nu_e}{8\sqrt{2}}\frac{\left(n_1^{\,2} - n_3^{\,2}\right)\left(n_2^{\,2} - n_3^{\,2}\right)}{\left(n_1^{\,2} + n_3^{\,2}\right)^{1/2}\left(n_2^{\,2} + n_3^{\,2}\right)^{1/2}\left\{\left(n_1^{\,2} + n_3^{\,2}\right)^{1/2} + \left(n_2^{\,2} + n_3^{\,2}\right)^{1/2}\right\}}$$

$$S^{LW} = \gamma\left(\cos\theta^e - 1\right)$$

$$\Delta G^{LW} = S^{LW}\left(\frac{d_0^{\,2}}{h^{e\,2}}\right)$$